Proceedings World Geothermal Congress 2015
Melbourne, Australia, 19-25 April 2015

The Influence of the Darcy Velocity of Groundwater Flow on the Effective Thermal Conductivity

Heiko Huber* and Ulvi Arslan

CDM Smith, Neue Bergstraße 13, 64665 Alsbach

heiko.huber@cdmsmith.com

Keywords: Geothermics, heat transport, experimental investigation, effective thermal conductivity, groundwater flow

ABSTRACT

An extensive database of groundwater influenced geothermal systems was developed through experimental investigation with a conduction and convection laboratory device. The experimental investigation focused on groundwater flow velocities and thermal loads with practical relevance, thereby acting a reasonable extension for the currently available measuring data concerning groundwater flow influenced geothermal systems. The transferability of the database to in-situ geothermal systems was proved via experimental investigation in two geothermal field testing sites. By the means of a numerical model, which was calibrated and validated with the experimental database, an extension of the experimental investigation range of middle to coarse sand was stretched out to cover silt, fine sand and gravel.

With the aid of this database, recommendations on the dimensioning of geothermal systems influenced by groundwater were developed. The correlation between the increase of the effective thermal conductivity of sands and the groundwater flow velocity was quantitatively determined and summarized in a tabular form for weakly aquiferous, aquiferous and strongly aquiferous sands. Therefore, it is possible to distinguish by practical engineering means between the effective thermal conductivities not only for dry, moist and water-saturated sand - according to common literature and national standards - but also for weakly aquiferous, aquiferous and strongly aquiferous sands, which in return contributes to the development of renewable energies.

1. INTRODUCTION

The multi-phase soil body consists of a solid phase, a liquid phase and a gaseous phase. Heat transport takes place in each of these phases through various mechanisms including conduction, convection, radiation and the interaction between the phases.

According to the state of art, soil is assumed to be a single-phase medium and not a multi-phase medium for both the on-field experiments and the laboratory experiments of the subsoil examination as well as for the numerical modeling. The mechanisms of heat transport for each of the individual phases are not recognized independently of one another, but are rather combined to form effective (or apparent) values such as the effective thermal conductivity. Especially for geothermal systems influenced by groundwater flow, the different heat transfer mechanisms of the liquid phase (the gas phase) and the solid phase as well as their interactions may not be neglected as to obtain reliable calculation results.

Various numerical studies have investigated the increase in the effective thermal conductivity of geothermal systems as a function of groundwater flow velocity. Accordingly, the proportion of heat transferred by convection to the total heat transport is due significantly to Darcy velocity higher than 0.01 m d^{-1} (Witte & van Gelder 2006; Pannike et al. 2006, Katsura et al. 2009). Different temperature measurements were performed in field test studies in order to determine the effective thermal conductivity (Palmer et al. 1992, Markle et al. 2006). However, the experimentally obtained measurement data on the proportion of heat transferred by convection to the total heat transfer as a function of groundwater flow velocity are not present sufficiently.

In order to optimize the dimensioning of geothermal systems, the increase of the effective thermal conductivity of geothermal systems by the groundwater flow velocity was determined through extensive laboratory experiments, field tests and a numerical study. Based on the results, recommendations were developed for the dimensioning of geothermal systems taking into account the Darcy velocity of the groundwater flow.

2. LABORATORY TESTS

A large-scale heat conduction and convection laboratory device was developed in order to investigate the increase of the effective thermal conductivity on geothermal systems as a function of groundwater flow velocity at the Technical University Darmstadt (Huber 2013).

The laboratory device was constructed in a large scale with inner dimensions of 297 cm / 64 cm / 71 cm (L / W / H) (Fig. 1). The construction is very massive with an acryl glass wall of 1.5 cm supported by a steel frame in a U 80 shape placed vertically at every 50 cm and horizontally at the top and the bottom. The device is covered by an acryl glass plate. The device can be filled with different kinds of water-saturated soil. With its massive construction, confined water of high pressure can be simulated. At the borders of the device, a connection for the water inlet and water outlet is installed. At the outside of the device, the water inlet is connected to a water supply tank of an adaptable height.

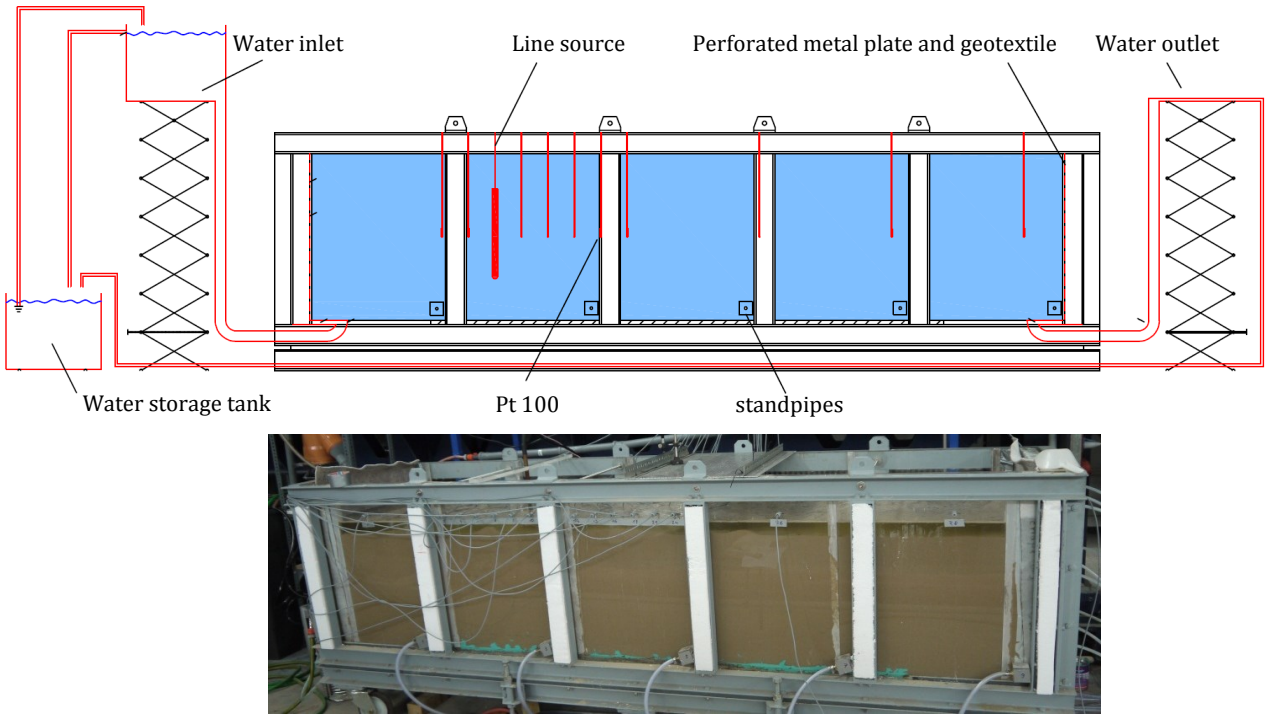

Figure 1: System sketch and photo of the developed laboratory device in front view

The water outlet is connected to a hydraulic pipeline, which is also variable in its installation height. Inside the device, the water inlet and outlet are enlarged to form diffusors of perforated metal plates and geotextiles being installed at a distance of 13.3 cm apart from each border. The diffusors release the water flow uniformly over the whole section of the device. According to the applied difference in height ΔH between the hydraulic head of the water supply tank and the pipelines at the water outlet, different flow velocities of the water running through the device can be regulated according to the permeability of the installed soil taking into consideration Darcy´s law.

A line source is installed vertically at about one third of the length of the device (83.3 cm). This line source is constructed from a copper tube with an outer diameter of 1.8 cm which is filled with silicon oil surrounding a heating element. With the aid of this line source, a thermal load can be applied to the installed soil, steady or transient in time. The laboratory device is thermally isolated with different layers of Styrofoam. A constantly tempered fluid circulates in copper tubes between these different layers of Styrofoam. Therefore, a desired constant temperature can be applied to the borders of the device.

The laboratory device is equipped with an extensive measuring system. The hydraulic head of the water supply tank, the water outlet pipelines and different points of the inside of the laboratory device are monitored with 12 water standpipes. In order to be able to compare the different hydraulic heads, the water standpipes are situated next to each other in a water harp.

Mass flow is measured constantly with flowmeters at the water inlet and the water outlet. At the water outlet, the whole section of the device is divided into 9 chambers of the same area with separated water outlets. The mass flow through these 9 chambers can be separately measured. Therefore, the homogeneity of the water flow over the whole section of the device can qualitatively be verified.

After all, 33 temperature sensors of Pt 100 are installed in or at the laboratory device in order to be able to constantly determine the development of temperature over time. Two Pt 100s are installed to measure the temperature of the flowing water at the water inlet and outlet. One sensor is installed inside the line source to guarantee an accurate thermal load. 30 Pt 100s are located in a horizontal section at the middle of the height of the device.

After all, 42 experimental scenarios were carried out with durations of at least two days and with varying thermal loads and Darcy velocities.

Figure 2 shows examples of the measured temperatures for a series of experiments (named Sz 1b) in which the laboratory device (here plan view) was filled with coarse sand and the thermal load was held constant at 23.3 W m^{-1} while the Darcy velocity v was varied between 0 m d^{-1} and 1.4 d m d^{-1}. The figure also shows the temperature variations at 6, 12 and 24 hour intervals preceding the application of the thermal load. Values of 20.1°C and 20.5°C highlight the isotherms. The shapes of the isotherms vary with increasing Darcy velocity from a circular to an elliptical shape with a ratio (a to b) ranging from 1 to 8.8. The shape coefficients (a and b) describe the length from the line source to the edge of the isotherm in the flow (a) or to the effluent (b) direction. The shapes of the detected elliptical temperature expansions coincide with the results of the analytical analysis. Based on the determined slope of the temperature increase insight, the line source the effective thermal conductivity can be determined depending on the Darcy velocity and using the Kelvin's theory. Further information on the performed laboratory tests is given in (Huber & Arslan 2013a).

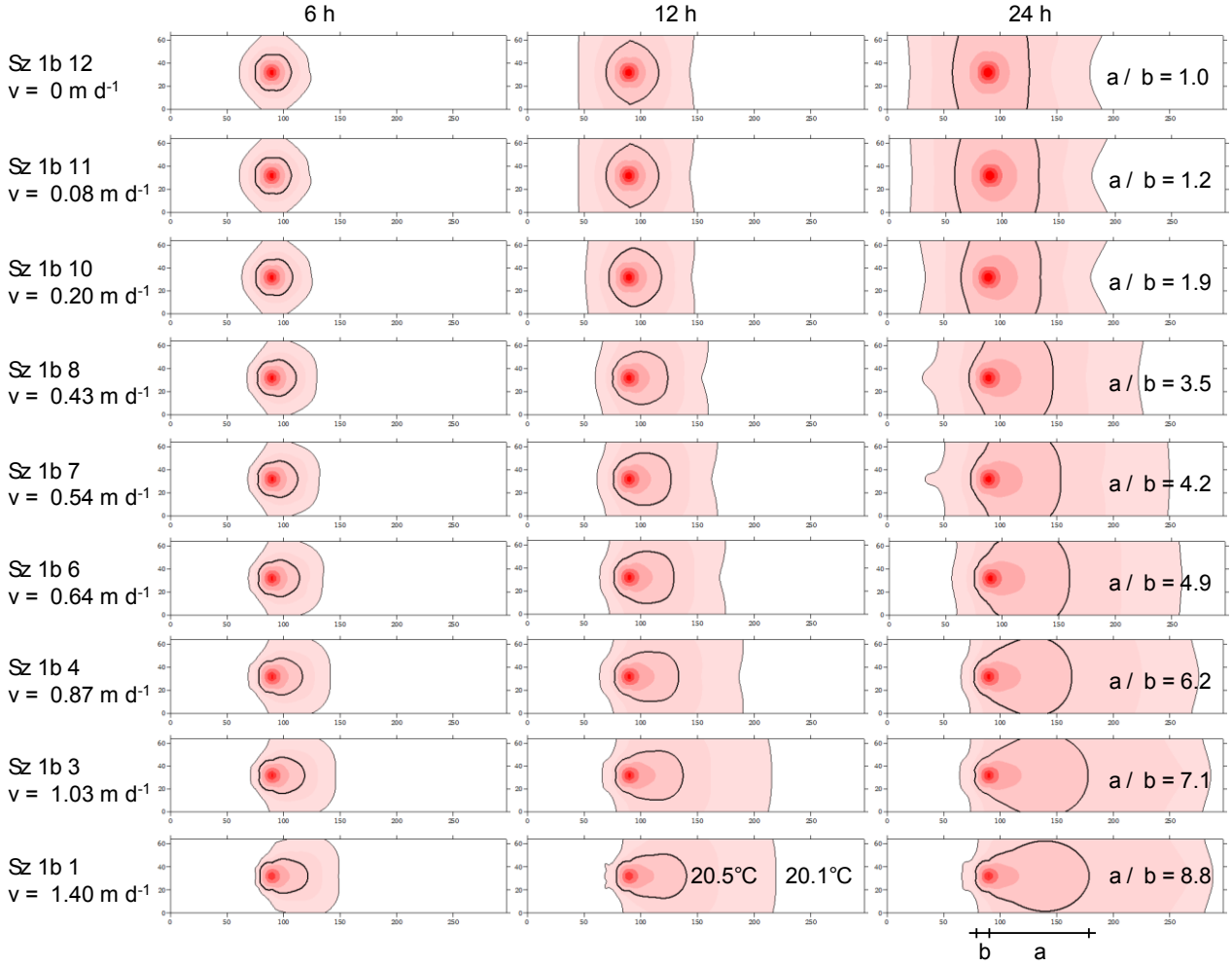

Figure 2: Measured temperature plumes depending on Darcy velocity (plan view) of a laboratory test scenario with 20.1°C and 20.5°C isotherms

3. FIELD STUDIES

To investigate the transferability of the results of the laboratory tests to geothermal systems under in-situ conditions, hydrogeological and geothermal field tests were carried out on two field testing sites being located in Darmstadt and Berlin Strausberg (Huber 2013). After all, four borehole heat exchangers (BHE) were constructed at the field testing site in Berlin Strausberg. The BHE named EWS 5 – EWS 8 have uniform lengths of 50 m each and were equipped with fiber optic cables.

Additionally, four groundwater standpipes named B 1 to B 4 were constructed with depths ranging from 31.0 m (B 1) to 37.0 m (B 4). The length of the filter sections at the base of groundwater standpipes varies between 3.0 m (B 1 - B 3) and 6.0 m (B 4). The filter slot width is uniformly 0.3 mm, while the filter gravel has a grain size of 1 mm to 2 mm. The four groundwater standpipes are located in one line according to the expected groundwater flow direction right before (B 2, B 3 and B 4) and behind (B 1) EWS 6 (Fig. 3). The distances between the groundwater standpipes and the borehole heat exchanger vary between 1.7 m to 7.9 m. The encountered geological conditions as a result of the performed investigation drillings are shown in Figure 4. Confined groundwater was encountered below the upper boulder clay layer with a hydraulic head of 10.8 m below surface (69.4 m asl). Due to the confined groundwater and the thin layer of marl at a depth of about 46.2 m – 47.5 m below ground, a nearly horizontal groundwater flow can be assumed for BHE 6 at the depth of 21.0 m – 46.2 m which is about 50 % of the whole length of the BHE (Fig. 4).

After the completion of the groundwater standpipes, two long-term pumping tests (PV 1 and PV 2) were carried out on site. The testing period was five days, each. The groundwater was withdrawn from the groundwater standpipe B 4 with constant flow rates of 3.4 $m^3 h^{-1}$ (PV 1) and 7.5 $m^3 h^{-1}$ (PV 2), respectively. During the stationary phase of the pumping tests, the hydraulic gradients at the borehole heat exchanger EWS 6 were found to be 0.017 (PV 1) and 0.029 (PV 2) using the measured energy levels of the confined groundwater at the groundwater standpipes B 1 and B 2. The permeability of the aquifer was determined in both the transient phase and in the stationary state to be $2.5 \cdot 10^{-5}$ m s^{-1} and $1.0 \cdot 10^{-4}$ m s^{-1}.

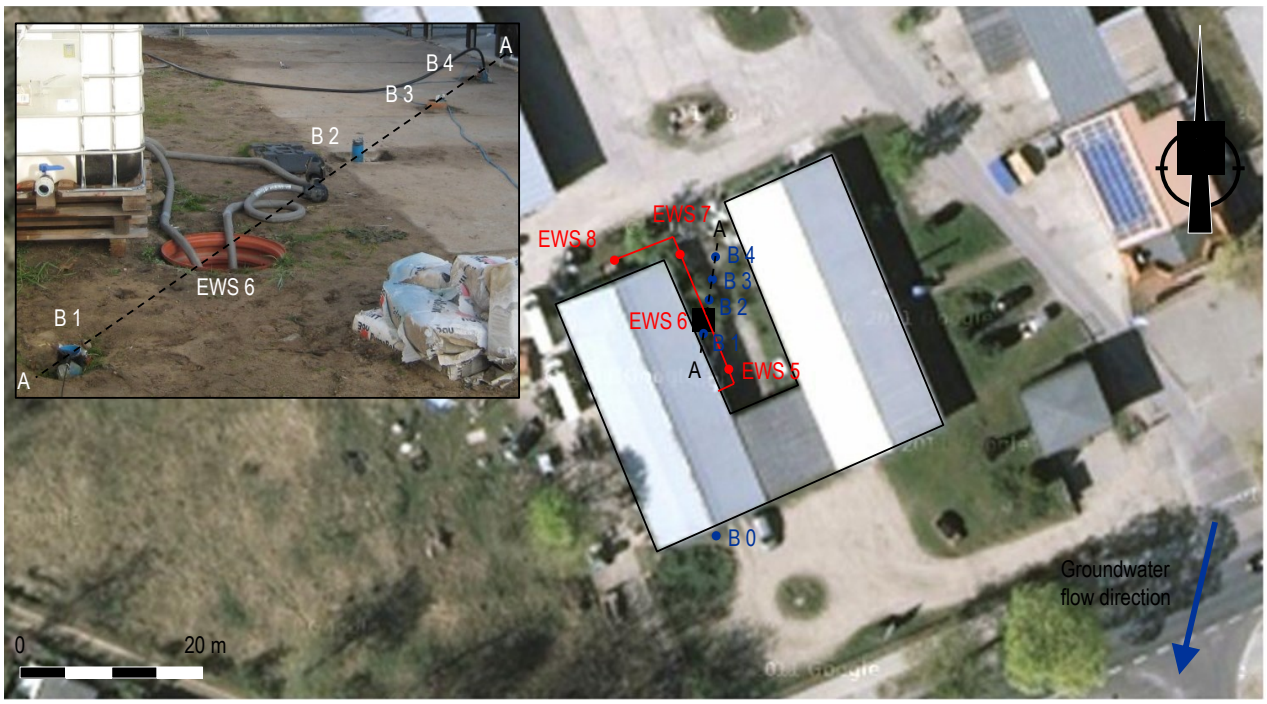

Figure 3: Field test site in Berlin Strausberg showing borehole heat exchangers EWS 5 – 8 and groundwater standpipes B 0 – B 5

At the groundwater standpipe B 2, three groundwater flow visualizations (GFV 1 - 3) were performed at B 2 by Phrealog. During a GFV measurement, a high resolution camera is located between two packers inside the filter pipe of a given groundwater standpipe. The camera recognizes suspended sediments transported by the groundwater and therefore, is able to determine the groundwater flow direction and velocity. Extensive information on the theoretical background of the GFV measurement is given in (Schöttler 1997). The aim of these hydrogeological investigations was to determine the depth related Darcy velocity of the groundwater flow as well its direction under natural and artificially-altered conditions in the immediate vicinity of borehole heat exchanger EWS 6. For this purpose, one GFV (GFV 1) was carried out under natural hydraulic conditions, while two GFV were performed under artificially altered groundwater flow velocities during the stationary phase of the pumping test of PV 1 (GFV 2) and PV 2 (GFV 3).

In GFV 1, the natural groundwater flow velocity and direction was determined at five different depths within the filter section between 34.0 m and 35.8 m below surface. The weighted average of the detected groundwater flow directions points to the south (175 °) correlating to the expected natural groundwater flow direction according to the hydrogeological map. The Darcy velocities determined vary between 0.09 m d^{-1} and 0.51 m d^{-1} with a weighted average value of 0.28 m d^{-1}. It is assumed that the natural groundwater flow velocity measured at the groundwater standpipe B 2 corresponds to the groundwater flow velocity at borehole heat exchanger EWS 6 which is located at a distance of about 2.7 m from B 2.

In both GFV 2 and GFV 3, the determined groundwater flow directions differ from the natural groundwater flow direction as determined in GFV 1 by approximately 180° (approximately to the north-northeast) at several depths and thus point in the direction of the groundwater standpipe B 4. However, due to the test results of GFV 2 and GFV 3, there were also groundwater flow directions determined which are not influenced by the groundwater extraction in B 4 and thus remains pointing to the supposed natural groundwater flow direction (south-southwest). This illustrates that the flow direction is not influenced by the pumping tests over the entire aquifer's thickness, but rather by the preferred groundwater flow pathways.

The determined Darcy velocity profiles of GFV 2 and GFV 3 qualitatively show the same pattern as determined in GFV 1. While the specific Darcy velocities determined in GFV 1 do not vary much over the filter section depth, significant groundwater flow velocity peaks appear in GFV 2 and GFV 3 at depths of 34.0 m, 34.5 m and 35.65 m below the surface. These velocity peaks correspond to the natural favored groundwater pathways within the aquifer.

The determined Darcy velocities at EWS 6 at depths between 34.0 m and 35.8 m below the surface were about 0.39 m d^{-1} while PV 1 and 0.7 m d^{-1} while PV 2. The increase of the artificially enlarged groundwater flow velocities while PV 1 (GFV 2) and PV 2 (GFV 3) compared to the natural groundwater flow velocity according to GFV 1 corresponds to the determined increase of the hydraulic gradient between B 1 and B 2 times the determined permeability of the groundwater aquifer.

Three geothermal response tests (GRT) were carried out at the borehole heat exchanger EWS 6 in combination with Enhanced Geothermal Response Tests (EGRT) in the period between July and November 2011. The heating power was thereby applied to the heat carrier fluid from EWS 6 using the GRT unit. The temporal development of the temperature at the U-tube inlet and outlet of EWS 6 were measured. Simultaneously, the temperature development over the whole depth of the EWS 6 was determined by means of fiber optic temperature measurement using the EGRT unit. While the thermal conductivity of a geothermal system can be determined only as an integral value over the depth by a GRT, the thermal conductivity of a geothermal system can be determined

by an EGRT over the whole length of the BHE. The advantage of combing GRT and EGRT is that the thermal conductivity of a geothermal system can be determined with two independent and different measurement systems and thus be compared.

While GRT 1 and EGRT 1 were performed with natural groundwater flow velocities, GRT 2 and EGRT 2 were performed while pumping test PV 1 and GRT 3 and EGRT 3 were performed while pumping test PV 2 under artificially enlarged groundwater flow velocity. After all, a clear correlation was proved between the increase of the depth related groundwater flow velocities (which was determined by groundwater flow visualization) and the increase of the depths related effective thermal conductivity (which was determined by the EGRT device).

The depths related effective thermal conductivities determined with EGRT 1 – 3 run qualitatively similarly to each other; they show more or less pronounced thermal conductivity peaks at the same depths (Fig. 4). Depending on the applied Darcy velocity of the groundwater, the detected average effective thermal conductivity increases from 2.11 W m^{-1} K^{-1} in EGRT 1 to 2.37 W m^{-1} K^{-1} (increase of 12.3 %) in EGRT 2 and to 2.49 W m^{-1} K^{-1} (increase of 18.0 %) in EGRT 3.

Within the upper 5 m below the surface, a high thermal conductivity value shows up in all three tests, which is mainly due to the influence of the outside temperatures.

A distinctive peak in the effective thermal conductivity at a depth of about 15 m below the surface was noticed within the upper marl layer in all three EGRTs. This peak is probably linked to heterogeneities within the marl layer, such as a region of higher density or preferred water pathways.

Furthermore, a distinct peak in the effective thermal conductivity was determined in all three EGRTs at the top of the water-bearing sand coal layer right at the base of the upper marl layer (about 21.5 m below the surface). This peak may be caused by the confined groundwater flowing along a favored pathway right below the glacial till. The highest increase of the effective thermal conductivity was determined in the section between 21.0 and 46.2 m b. surface which is the region where the main groundwater flow occurs. In this section an increase of the effective thermal conductivity of 13.3 % (EGRT 2, while v = 0.39 m d^{-1}) respectively of 21.9 % (EGRT 3, while v = 0.70 m d^{-1}) was determined compared to the results of EGRT 1 (while v = 0.28 m d^{-1}). According to preferred groundwater flow pathways in the aquifer, an increase in the effective thermal conductivity $\lambda_{eff}(z = 34\ m)$ in a depth of 34 m of even 16.6 % (EGRT 2) and 32.2 % (EGRT 3) compared to EGRT 1 was observed. The depth of this section of the maximum increase of the effective thermal conductivity correlates with the depth of the maximum groundwater flow velocity determined in GFV 2 and GFV 3, which is about of 34 m below the surface, also corresponding to the middle of the filter section of B 4.

At a depth range between about 42 m and 50 m below surface, the effective thermal conductivity decreases significantly. This is justified by the fact that no distinctive groundwater flow is present in this region due to the low permeability of the boulder clay layer at 46.2 m below the surface.

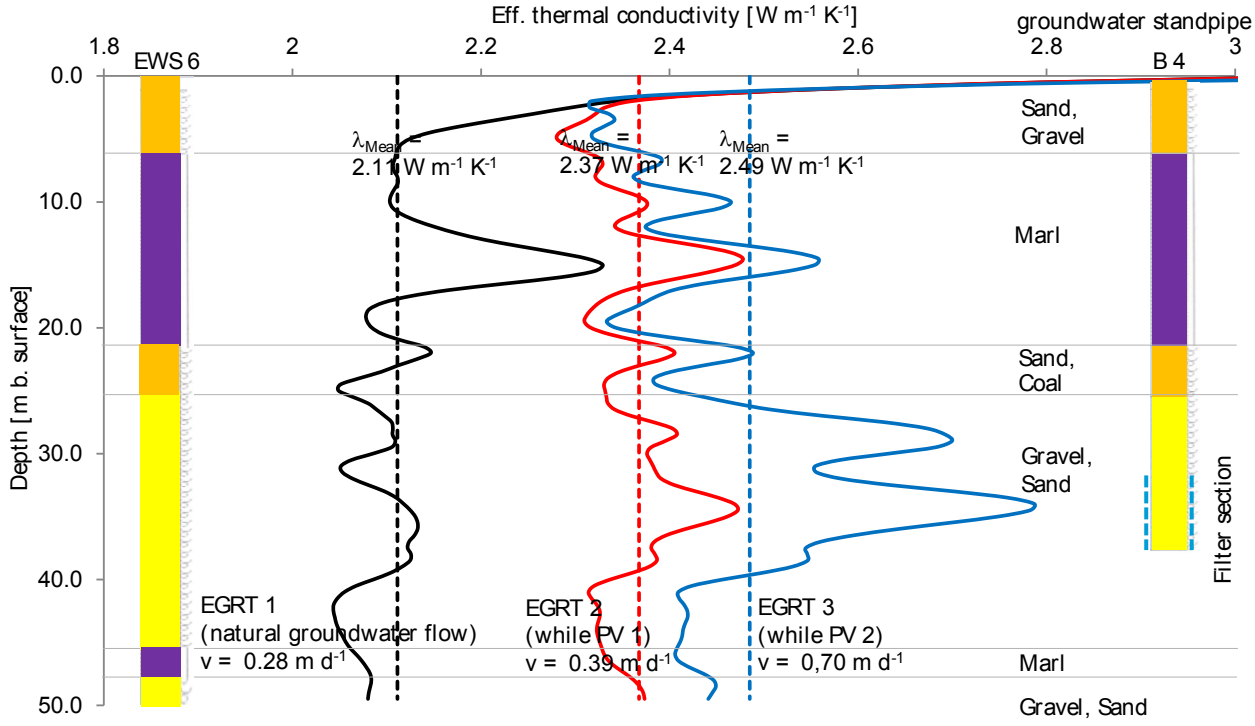

Figure 4: Field test site in Berlin Strausberg – Geological section and results of EGRT 1 - 3

Within the conducted field studies, a clear correlation between the detected groundwater flow velocities and the determined effective thermal conductivities at the borehole heat exchanger EWS 6 was noticed. By artificially increasing the groundwater flow velocities, a maximum increase of the effective thermal conductivity of up to 32.2 % could be achieved. Overall, the results confirm that the experimental procedure was consistent. The field stand test at Strausberg provides reliable data on the effective thermal

conductivities of a geothermal system as a function of groundwater flow velocity. Thus, the findings obtained in the laboratory device can be applied to real geothermal systems. Further information on the performed field tests is given in (Huber & Arslan 2013b).

4. NUMERICAL INVESTIGATIONS

The experimental geothermal data gathered in laboratory tests as well as in field tests were back analyzed with numerical methods (Huber 2013). The numerical back analysis was performed with FEFlow 6.0 by DHI WASY, a finite-element-method based code for combined transient heat and transient flow transport simulation. The laboratory device was simulated as a two dimensional, horizontal, water saturated problem, while the model area corresponds to the sensor area, which is located in the half of the height of the laboratory device.

The simulation area was discretized with more than 130,000 three-nodded triangles with a higher density of elements inside and right beside the line source and at the borders of the simulation area. The duration of the simulation was chosen according to the performed scenarios to be two days, each. The automatic time stepping control scheme was chosen as the predictor-corrector Adams-Bashforth / Trapezoid rule.

The modeling area was simulated with three different materials. Material 1 defines the water-saturated soil inside the laboratory device, material 2 and material 3 describes the line source simulated as copper tube (material 2) which is filled with silicon oil (material 3). As initial conditions the temperature of the laboratory device was set to 20°C and the hydraulic head was set at 0.3 m above the height of the laboratory device. As boundary conditions, the hydraulic heads of the diffusors were defined as constant and the temperature of the border and the diffusors were also set constant.

While most of the values of the water saturated-sand (material 1) were determined in laboratory, the values of the copper tube (material 2) and the silicon oil (material 3) were chosen based on common literature references. The thermal conductivity and the permeability of the silicon oil were chosen to be of very high values to guarantee a fast distribution of the temperature inside the line source. The thermal conductivity of the copper tube was chosen to be very low, as to simulate the heat transfer from the flowing silicon oil to the copper tube and from the copper tube to the water-saturated sand with flowing groundwater.

Table 1: Properties of the materials 1 - 3

	unit	*bandwidth*	*standard value*	*remark*
Water saturated soil (material 1)				
Thermal conductivity of solid λ_S	W m^{-1} K^{-1}	2.5 – 6.0	3.85	determined in laboratory
Thermal conductivity of fluid λ_F	W m^{-1} K^{-1}	0.597	0.597	determined in laboratory
Vol. heat capacity of solid c_S	MJ m^{-3} K^{-1}	1.0 – 2.5	1.73	determined in laboratory
Vol. heat capacity of fluid c_F	MJ m^{-3} K^{-1}	4.18	4.18	determined in laboratory
Porosity n	-	0.4 – 0.5	0.46	determined in laboratory
Permeability k	m s^{-1}	$3.8 \cdot 10^{-3}$	$3.8 \cdot 10^{-3}$	determined in laboratory
Dispersivity α_L / α_T	m / m	0/0 – 0.25/0.025	0/0	according to common literature
Darcy velocity v	m d^{-1}	0 – 0.46	0.155	determined in laboratory
Copper tube (material 2)				
Thermal conductivity of solid λ_S	W m^{-1} K^{-1}	0.05 – 0.07	0.056	according to common literature
Vol. heat capacity of solid c_S	MJ m^{-3} K^{-1}	0.03 - 300	3.45	according to common literature
Porosity n	-	0	0	according to common literature
Permeability k	m s^{-1}	$1.0 \cdot 10^{-20}$	$1.0 \cdot 10^{-20}$	according to common literature
Silicon oil (material 3)				
Thermal conductivity of fluid λ_F	W m^{-1} K^{-1}	5 - 100	100	according to common literature
Vol. heat capacity of fluid c_F	MJ m^{-3} K^{-1}	1 - 40	10	according to common literature
Porosity n	-	1	1	according to common literature
Permeability k	m s^{-1}	1	1	according to common literature

The influence of the property of every single material was investigated with help of a numerical sensitivity analysis. While all other properties were set to the standard values, one property was varied between the chosen bandwidth according to (Table 1). The results of the sensitivity analysis are summarized in (Fig. 5 and Fig. 6). The continuous blue line shows the (in the laboratory test measured) temperature development of the temperature sensor inside the line source gathered in the experiment numbered Sz 3a 5.

A variation of the thermal conductivity λ, the heat capacity c and the porosity n of the water-saturated sand lead to a parallel displacement of the temperature increase with only small variation of the slope of the temperature increase. The slope of the temperature increase without a parallel displacement varies depending on the simulated Darcy velocity v (Fig. 5).

A variation of the thermal dispersivity of the water-saturated sand leads only to a small parallel displacement of the slope of temperature increase. This is caused due to the small dimensions of the laboratory device. The thermal dispersivity only affects the temperature development in field experiments with larger dimensions.

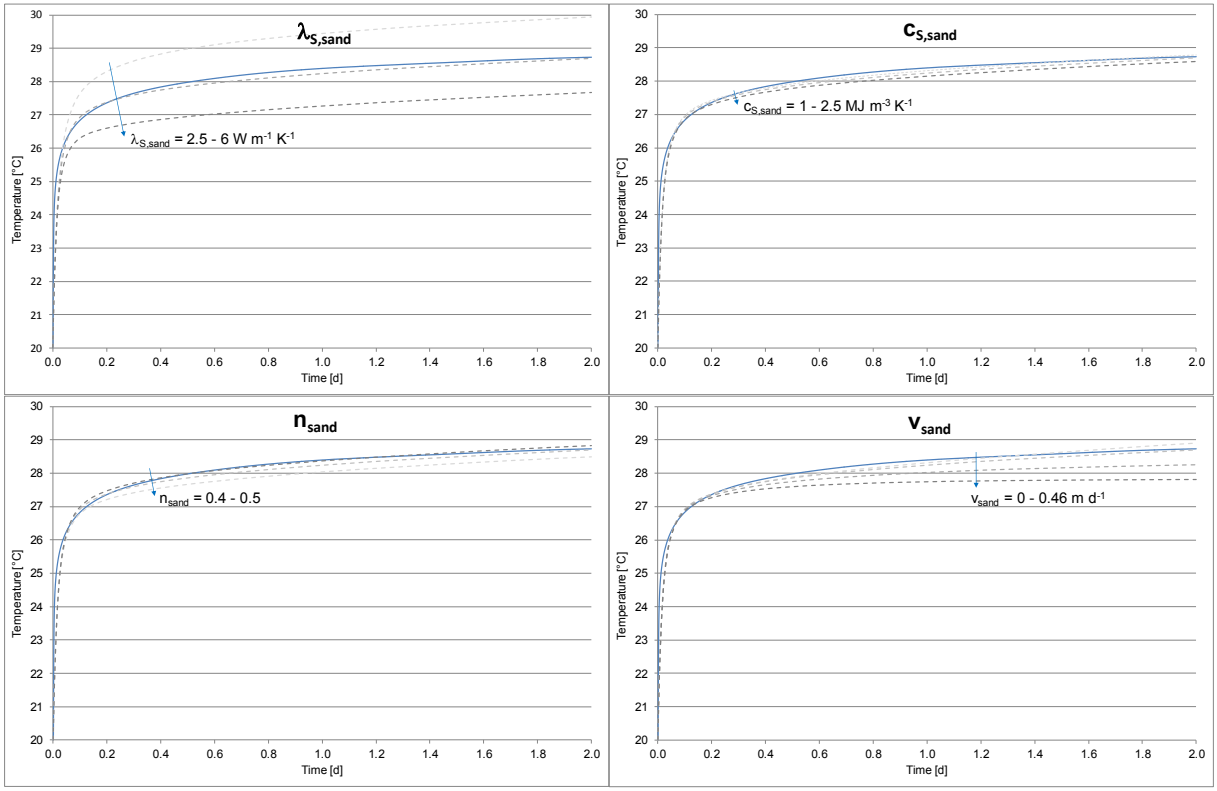

Figure 5: Sensitivity analysis – variation of λ_S, c_S, n and v of material 1 (sand)

A variation of the thermal conductivity λ of the copper tube and the silicon oil lead to a parallel displacement of the temperature increase with only small variation of the slope of the temperature increase. A variation of the heat capacity of the copper tube and the silicon oil lead to a displacement of the temperature increase at the beginning of the thermal load. The temperature retains longer inside the line source due to a higher heat capacity. This leads to higher temperatures at the beginning of the experiment (Fig. 6).

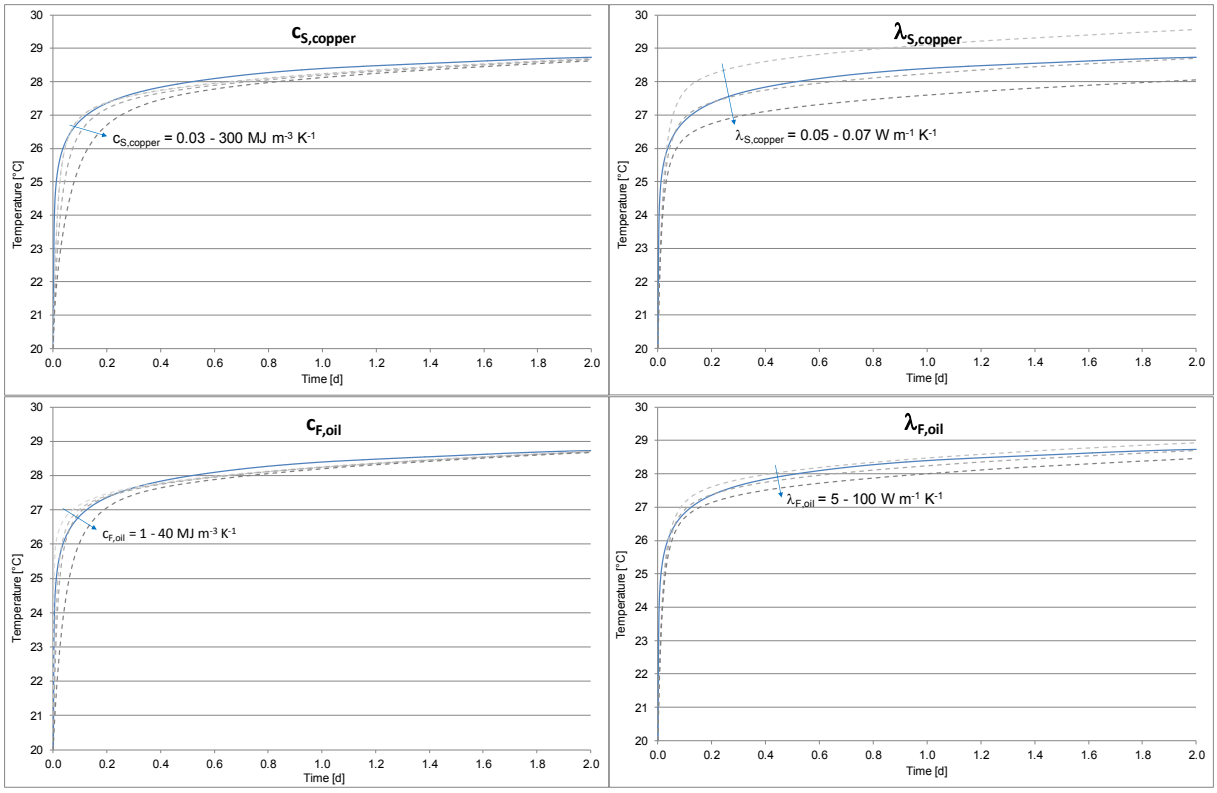

Figure 6: Sensitivity analysis – variation of c_S and λ_S of material 2 (copper) and c_F and λ_F of material 3 (oil)

After all, a good fit of the numerical back analysis to the experimental laboratory data was achieved and the numerical model was calibrated for the scenario Sz 3a 5. To validate the numerical model, the scenarios Sz 3a 7 – Sz 3a 10 were back analyzed. In the experimental laboratory scenarios of Sz 3a 7 – Sz 3a 10, all of the geological and hydro geological values were kept constant, while only the thermal load applied on the line source was varied between 14.8 W m^{-1} (Sz 3a 8) and 40.1 W m^{-1} (Sz 3a 9). Due to the variation of the constant thermal load, the temperature inside the line source increases to values of 26°C – 36°C after two days.

Furthermore, a second validation of the numerical model was performed with the aid of the scenarios Sz 1b 3 - Sz 1b 11. In the experimental laboratory scenarios all of the geological values as well as the thermal load applied were kept constant, while only the Darcy velocity was varied between 0.05 m d^{-1} (Sz 1b 11), 0.20, 0.43, 0.54, 0.74 and 1.03 m d^{-1} (Sz 1b 3). Due to the variation of the Darcy velocity, the temperature inside the line source increases to values of 25°C – 27°C after two days.

A comparison of the temperatures inside the line source according to the experimental laboratory data (continuous red lines) and the numerical back analysis (dashed grey lines) for the scenarios Sz 3a 7 – Sz 3a 10 (left) and Sz 1b 3 – Sz 1b 11 (right) is shown in (Fig. 7). After all a good fit of the numerical back analysis to the experimental laboratory data was achieved.

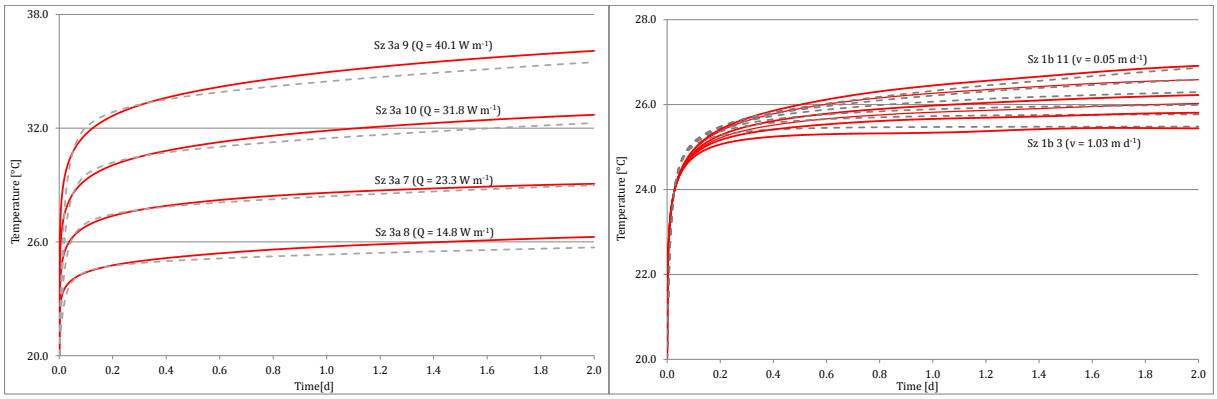

Figure 7: Comparison of the experimental laboratory data with the data from the numerical back analysis

The numerical model was calibrated and validated with aid of different scenarios of the laboratory tests. With the validated numerical model, an extrapolation of the gathered experimental data was performed. Therefore, the properties of material 1 (installed sediment) were varied from the determined or estimated values of the sand to properties of gravel, silt and clay according to common literature. With the aid of the numerical analysis it was possible to extrapolate the experimental data range from middle and coarse sand to fine sand, silt, clay and gravel. The results can be summarized as follows:

For the grain size of fine sand, a variation of the groundwater flow velocity in the typical range for those materials with low permeability (0 m d^{-1} - 0.1 m d^{-1}) show quiet low increase of the effective thermal conductivity. For the soil types with weak to very weak permeability such as silt or clay, the groundwater flow velocity has no influence on the temperature gradients of the line source and therefore on the thermal conductivity during the simulation period of two days. For grain sizes ranging from coarse sand to gravel a clear dependence of the effective thermal conductivity on the groundwater flow velocity was noticed.

5. CONCLUSION

Common literature as well as national standards (namely VDI 4640) distinguishes between the effective thermal conductivities for dry, moist and water-saturated sands. The influence of the Darcy velocity on the increase of the effective thermal conductivity is not considered in these recommendations so far.

Therefore, extensive experimental investigation in laboratory tests, field tests and numerical extrapolation were performed to investigate the increase of the effective thermal conductivity of water saturated sediments in dependence of the groundwater flow velocity. A database of groundwater flow influenced geothermal systems was established by experimental investigation with a developed laboratory device. The transferability of the database to geothermal systems in-situ was proved via experimental investigation in two geothermal field testing sites. By the means of a numerical model, which was calibrated and validated with the experimental database, an extrapolation of the experimental investigation range of middle to coarse sand was stretched out to cover silt, fine sand and gravel.

In summary of the results of laboratory tests, field tests and numerical investigations executed, a more or less significant influence of the groundwater flow velocity on the increase of the effective thermal conductivity could be observed depending on the investigated grain size. For grain sizes ranging from middle sand to coarse sand and gravel, a clear dependence of the effective thermal conductivity on the Darcy velocity was noticed even at small velocities in the bandwidth typical for those sediments. For the grain size of fine sand, a variation of the groundwater flow velocity in the typical range for those sediments with low permeability (0 m d^{-1} - 0.1 m d^{-1}) showed a quiet low increase of the effective thermal conductivity. For the soil types with weak to very weak permeability such as silt or clay, the groundwater flow velocities had no influence on the temperature gradients of the line source and therefore on the thermal conductivity during the simulation period of two days.

After all, there is an exponential correlation between the increase of the effective thermal conductivity of water-saturated sands and the groundwater flow velocity, Fig 8. The effective thermal conductivity of a water-saturated sand with Darcy velocities up to 0.3 m d^{-1} (weakly aquiferous) can increase up to 25 %, an aquiferous sand (Darcy velocity 0.3 m d^{-1} – 0.6 m d^{-1}) leads to an increase of the effective thermal conductivity of up to 50 %. For water-saturated strongly aquiferous (0.6 m d^{-1} – 1.0 m d^{-1}) sand, an increase of the effective thermal conductivity up to 100 % can be expected (Fig. 8).

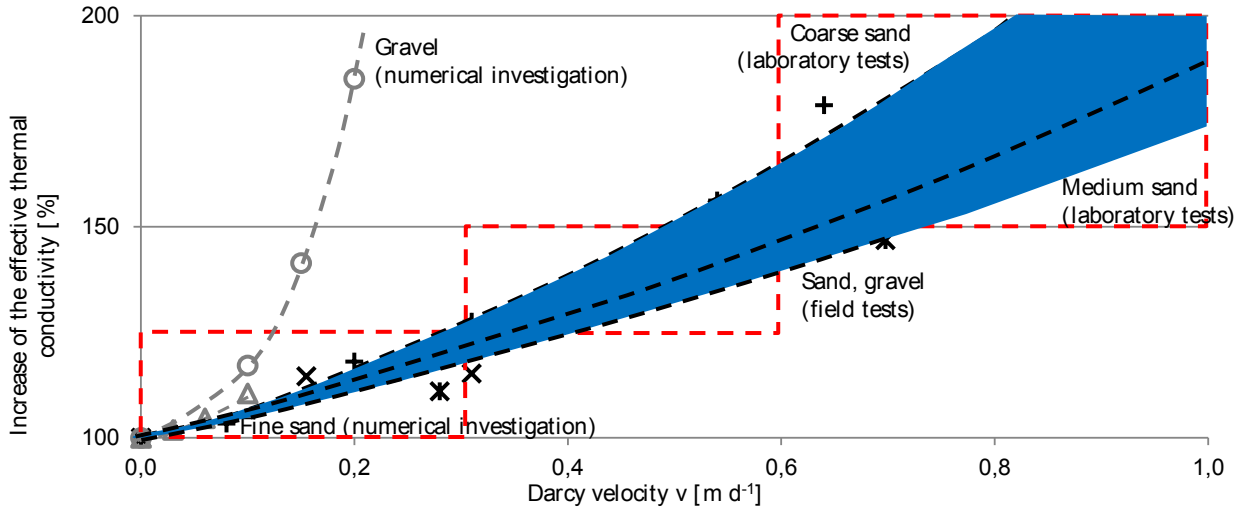

Figure 8: Increase of the effective thermal conductivity of different water saturated sediments in dependence of the Darcy velocity

In (Table 2), the recommended values for the effective thermal conductivities for water-saturated sands considering the Darcy velocity of the groundwater flow are assigned for weakly aquiferous (v = 0 m d^{-1}– 0.3 m d^{-1}), aquiferous (v = 0.3 m d^{-1}– 0.6 m d^{-1}) and strongly aquiferous (v = 0.6 m d^{-1} – 1.0 m d^{-1}) sands (Huber 2013).

Table 2: Increase of the effective thermal conductivity of water saturated sands in dependence of the Darcy velocity

Type of sand	*Darcy velocity v [m d^{-1}]*	*Thermal cond. λ_{eff} (recommended value) [W m^{-1} K^{-1}]*
dry, acc. to (VDI 4640)	0.0	0.4
moist, acc. to (VDI 4640)	0.0	1.4
water-saturated, acc. to (VDI 4640)	0.0	2.4 (reference)
weakly aquiferous	0.0 - 0.3	2.7 (+ 0 % - 25 %)
aquiferous	0.3 - 0.6	3.3 (+25 % - 50 %)
strongly aquiferous	0.6 - 1.0	4.4 (+ 50 % - 100 %)

With the aid of the determined effective thermal conductivities of water-saturated sands and whilst considering the groundwater flow, the dimensioning of the geothermal systems can be optimized.

REFERENCES

Huber, H.: Experimentelle und numerische Untersuchungen zum Wärmetransportverhalten oberflächennaher, durchströmter Böden. Dissertation, Mitteilungen des Instituts für Werkstoffe und Mechanik im Bauwesen, Heft 40, Darmstadt, 2013

Huber, H., Arslan, U.: (a) Characterization of heat transport processes in geothermal systems, International Journal of Low-Carbon Technologies 2013; doi: 10.1093/ijlct/ctt014

Huber, H., Arslan, U.: (b) Numerical Back-Analysis of Geothermal Laboratory Tests with Forced Groundwater Flow, Thirty-Eighth Workshop on Geothermal Reservoir Engineering Stanford University, Stanford, California, 11.02.-13.02.2013

Katsura, T., K. Nagano, S. Hori und T. Okawada. 2009. Investigation of groundwater flow effect on the thermal response test result. Proceedings 11th Energy Conservation Thermal Energy Storage Conference Effstock 2009, Stockholm.

Markle, J.M., Schincariol, R.A., Sass, J.H., Molson, J.W.: Characterizing the two-dimensional thermal conductivity distribution in a sand and gravel aquifer. Soil Science Society of America Journal, 70(4): (2006), 1281-1294

Palmer, C.D., Blowes, D.W., Frind, E.O., Molson, J.W.: Thermal-Energy Storage in an Unconfined Aquifer .1. Field Injection Experiment. Water Resources Research, 28(10): (1992) 2845-2856.

Pannike, S., M. Kölling, H. D. Schulz, B. Panteleit, J. Reichling und V. Scheps. 2006. Auswirkung hydrogeologischer Kenngrößen auf die Kältefahnen von Erdwärmesondenanlagen in Lockersedimenten. Grundwasser 11(1): 6-18.

Schöttler, M. 1997. Meßbarkeit der Grundwasserbewegung durch Visualisierung der Strömung in Bohrbrunnen. Aachen.

VDI-4640. 2001. Thermal use of the underground – fundamentals, approvals, environmental aspects. (part 1) Berlin, Beuth.

Witte, H. J. L. und van Gelder, A. J.: Geothermal Response Tests using controlled multi-power level heating and cooling pulses (MPL-HCP): quantifying ground water effects on heat transport around a borehole heat exchanger. Proceedings of Ecostock, The 10th International Conference on Thermal Energy Storage, New Jersey, U.S.A. (2006)